

Model-Independent Analysis of the Indirect Effects of an Additional Z' -Boson at CLIC

D. V. Sinegribov,^{1,*} V. V. Andreev,^{1,†} and I. A. Serenkova^{2,‡}

¹*Francisk Skorina Gomel State University, 104 Sovetskaya Str, 246028 Gomel, BELARUS*

²*Sukhoi Gomel State Technical University,
48 October Ave., 246746 Gomel, BELARUS*

(Received 19 September, 2024)

In this paper, we present a technique for analyzing the indirect manifestation of an additional Z' -boson in the planned experiments at future e^+e^- colliders. The developed technique is based on the representation of the differential cross section for the process $e^+e^- \rightarrow \bar{f}f$ (where $f \neq e$) incorporating new effective parameters of the Z' -boson. The availability of the electron polarization option plays a key role in the implementation of the technique. As a result, we obtained model-independent constraints on the characteristics of the Z' -boson, taking into account the experimental capabilities of CLIC.

PACS numbers: 12.60.Cn, 13.66.De, 14.70.Pw

Keywords: Compact Linear Collider, beyond the Standard Model, Z' gauge boson

DOI: <https://doi.org/10.5281/zenodo.15081470>

1. Introduction

The Compact Linear Collider (CLIC) offers high-energy e^+e^- collisions up to center-of-mass energies of 3 TeV [1]. At the initial energy stage $\sqrt{s} = 380$ GeV, we have uniquely rich programme of Higgs and top-quark physics. At the higher-energy stages 1.5 TeV and 3 TeV, CLIC encompasses effects of beyond the Standard Model (SM). For this energies stages, we have 2.5 ab^{-1} and 5 ab^{-1} very high integrated luminosity, respectively. Polarization plays a key role in future electron-positron and hadron collider experiments [1, 2]. The CLIC baseline has $\pm 80\%$ longitudinal electron polarization and no positron polarization. The combined analysis of future data from the CLIC with data from the Large Hadron Collider (LHC) is also a point of interest [3]. Searches for new particles is one of the basic parts of the CLIC experimental program. In

this paper, we focus on the additional Z' -boson (Z') [4, 5]. Presently, we have no experimental indications for such particle [6].

We assume that the effective gauge group of a typical Z' model is

$$SU(3)_C \times SU(2)_L \times U(1)_Y \times U'(1), \quad (1)$$

where SM is supplemented by an additional $U'(1)$ gauge group [7–12]. The reason for the appearance of the Z' is symmetry breaking at energies of the order of TeV.

Grand unified theories predict many new particles, such as exotic fermions, additional charged gauge bosons or additional Higgs bosons. The number of exotic fermions increases significantly with the size of the gauge group. We shall ignore the couplings to other beyond-SM particles such as exotic fermions.

The general interaction Lagrangian for the gauge group (1) has the form:

$$\begin{aligned} \mathcal{L}_{NC} &= \frac{\delta_{Z'}}{2} Z'_\mu \bar{f} \gamma^\mu \left(g_v^f(Z') - g_a^f(Z') \gamma_5 \right) f \\ &= \sum_{\alpha=\pm} \delta_{Z'} Z'_\mu \bar{f} \gamma^\mu g_{Z',f}^\alpha \omega_\alpha f, \end{aligned} \quad (2)$$

where $\omega_\pm = (1 \pm \gamma^5)/2$ and the Z' couplings ($\delta_{Z'}$,

*E-mail: dvsinegribov@gmail.com; Also at Sukhoi Gomel State Technical University, 48 October Ave., 246746 Gomel, BELARUS

†E-mail: vik.andreev@gsu.by

‡E-mail: inna.serenkova@gmail.com

$g_{v,a}^f(Z')$ and $g_{Z',f}^\pm$) depend on the choice of the $U'(1)$.

Taking into account the actual bounds on the $M_{Z'} \sim 4 - 5$ TeV [13–16], we can study only indirect (or virtual) effects of the Z' at CLIC. We describe such effects as deviations from the prediction of the SM [17].

If a Z' is indeed discovered, possibly at hadron collider, precise measures of Z' couplings at CLIC would be essential for testing extended gauge models. In this regard, the primary focus is to obtain model-independent constraints on the Z' couplings and to investigate the sensitivity of the process $e^+e^- \rightarrow \bar{f}f$ to the chiralities λ_e and λ_f . To achieve the goal, we propose a technique (Sec. 5) that is based on the differential cross-section representation (Sec. 4). Linear dependence of this representation on the new effective parameters allows to get constraints using a combination of polarized observables. As a result, we obtained model-independent constraints on the left- and right-handed couplings of the Z' for 2 high energy energy stages at CLIC (Sec. 6). Such constraints can be used in the model-dependent analysis. The statistical processing plays a very important role in a such research. Often, correlation is not taken into account. Our technique takes into account the correlation. Note that the mass mixing of $Z - Z'$ bosons [18–20] is not taken into account in this paper.

2. Kinematics

We discuss a case of $f \neq e$ in the process

$$e^-(p_1, \lambda_{p_1}) + e^+(p_2, \lambda_{p_2}) \rightarrow f(k_1, \lambda_{k_1}) + \bar{f}(k_2, \lambda_{k_2}), \quad (3)$$

where four-momentum p_i^μ have the form:

$$p_1^\mu = \frac{\sqrt{s}}{2}(\gamma_{ij}, 0, 0, \beta_{ij}), \quad p_2^\mu = \frac{\sqrt{s}}{2}(\gamma_{ji}, 0, 0, -\beta_{ij}), \quad (4)$$

$$P^\mu = p_1^\mu + p_2^\mu = \sqrt{s}(1, 0, 0, 0). \quad (5)$$

In the (4), β_{ij} and γ_{ij} are

$$\beta_{ij} = \beta_{m_i^2, m_j^2}(s) = \sqrt{1 + (x_i^2 - x_j^2)^2 - 2(x_i^2 + x_j^2)}, \quad (6)$$

$$\gamma_{ij} = \gamma_{m_i^2, m_j^2}(s) = 1 + x_i^2 - x_j^2, \quad x_i = m_i/\sqrt{s}. \quad (7)$$

where $m_{i,j}$ is the fermion masses.

In case of $m_{i,j} = m_e$, the vectors (4) have the form:

$$p_1^\mu = \frac{\sqrt{s}}{2}(1, 0, 0, \beta_e), \quad p_2^\mu = \frac{\sqrt{s}}{2}(1, 0, 0, -\beta_e). \quad (8)$$

In case of $m_{i,j} = m_f$, we have, respectively:

$$k_1^\mu = \frac{\sqrt{s}}{2}(1, \beta_f \sin \theta \cos \phi, \beta_f \sin \theta \sin \phi, \beta_f \cos \theta),$$

$$k_2^\mu = \frac{\sqrt{s}}{2}(1, -\beta_f \sin \theta \cos \phi, -\beta_f \sin \theta \sin \phi, -\beta_f \cos \theta), \quad (9)$$

where \sqrt{s} is the center-of-mass energy, $\beta_f = \sqrt{1 - 4m_f^2/s}$ is the velocity of the final state fermion in the center-of-mass and θ is the angle between outgoing anti-fermion \bar{f} and incoming positron e^+ .

3. Amplitude

The process (3) at the Born level is described by s-channel Feynman diagram, shown in the Fig. 1.

The amplitude of this diagram is written as follows:

$$\begin{aligned} & \mathcal{M}_{\lambda_{k_1}, \lambda_{k_2}}^{\lambda_{p_1}, \lambda_{p_2}}(V) \\ &= (-1) \frac{\delta_V}{s} R_V \left(g^{\mu\nu} - \frac{P^\mu P^\nu}{M_V^2} \right) \sum_{\alpha_1, \alpha_2 = \pm} g_{V,e}^{\alpha_1} g_{V,f}^{\alpha_2} \\ & \times \bar{v}_{\lambda_{p_2}}(p_2) \gamma_\mu \omega_{\alpha_1} u_{\lambda_{p_1}}(p_1) \bar{u}_{\lambda_{k_1}}(k_1) \gamma_\nu \omega_{\alpha_2} v_{\lambda_{k_2}}(k_2), \end{aligned} \quad (10)$$

where $R_V = s/(s - M_V^2 + iM_V\Gamma_V)$ is the vector boson propagator, δ_V is the gauge coupling,

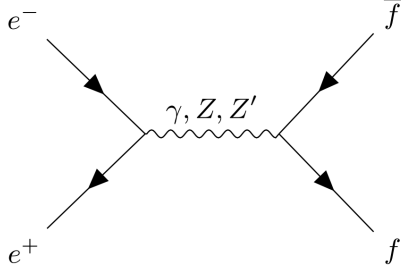


FIG. 1: Feynman diagram of the process (3).

Γ_V is the total decay width and M_V is the mass of vector boson V . The bispinors $u_{\lambda_{p_1}}(p_1)$ and $v_{\lambda_{k_2}}(k_2)$ satisfy Dirac equations and spin conditions for massive fermion and anti-fermion.

The couplings of the left- (L, -) or right- (R, +) handed fermion to the SM vector bosons are defined as:

$$g_{\gamma,f}^{\lambda_f} = -Q_f, \lambda_f = \pm, \quad (11)$$

$$g_{Z,f}^{\lambda_f} = \frac{(T_{3f} \delta_{-, \lambda_f} - Q_f \sin^2 \theta_W)}{\sin \theta_W \cos \theta_W},$$

where Q_f is the charge of fermion, T_{3f} is the third component of the SM isospin and θ_W is the Weinberg–Salam angle.

We use the original technique [21] to derive the compact form of the amplitude for all possible spin variables:

$$\mathcal{M}_{\lambda_{k_1}, \lambda_{k_2}}^{\lambda_{p_1}, \lambda_{p_2}}(V) = 2\delta_V R_V \left\{ \lambda_{k_1} \lambda_{p_1} \delta_{\lambda_{k_2}, \lambda_{k_1}} \delta_{\lambda_{p_2}, \lambda_{p_1}} g_a^f(V) g_a^e(V) \tilde{\eta}_f \tilde{\eta}_e \times \left(\frac{s}{M_V^2} - 1 \right) \right. \\ \left. + \left(\tilde{g}_{\lambda_{k_1}}^f(V) \delta_{\lambda_{k_2}, -\lambda_{k_1}} + g_v^f(V) \delta_{\lambda_{k_2}, \lambda_{k_1}} \tilde{\eta}_f \right) \left(\tilde{g}_{\lambda_{p_1}}^e(V) \delta_{\lambda_{p_2}, -\lambda_{p_1}} + g_v^e(V) \delta_{\lambda_{p_2}, \lambda_{p_1}} \tilde{\eta}_e \right) D_{\lambda_{p_1}, \lambda_{k_1}}^*(\phi, \theta, -\phi) \right\}, \quad (12)$$

where

$$\tilde{g}_\lambda^i(V) = g_v^i(V) - \lambda \beta_i g_a^i(V), \quad (13)$$

$$\eta_i = \frac{m_i}{\sqrt{s}}, \quad \tilde{\eta}_i = \sqrt{\frac{2}{s}} m_i, \quad i = e, f, \quad (14)$$

$$\lambda_{p_{12}} = (\lambda_{p_1} - \lambda_{p_2})/2, \quad \lambda_{k_{12}} = (\lambda_{k_1} - \lambda_{k_2})/2, \quad (15)$$

and $g_v^f(V) = \frac{1}{2}(g_{V,f}^- + g_{V,f}^+)$, $g_a^f(V) = \frac{1}{2}(g_{V,f}^- - g_{V,f}^+)$ are the vector and axial fermion couplings, respectively.

For the case $m_e \ll \sqrt{s}$, the amplitude (12) can be represented as:

$$\mathcal{M}_{\lambda_{k_1}, \lambda_{k_2}}^{\lambda_{p_1}, \lambda_{p_2}}(V) = 2\delta_{\lambda_{p_2}, -\lambda_{p_1}} D_{\lambda_{p_1}, \lambda_{k_1}}^*(\phi, \theta, -\phi) \\ \times \left(\delta_{\lambda_{k_2}, -\lambda_{k_1}} \tilde{g}_{\lambda_{k_1}}^f(V) + g_v^f(V) \delta_{\lambda_{k_2}, \lambda_{k_1}} \tilde{\eta}_f \right) g_{V,e}^{\lambda_{p_1}} \delta_V R_V, \quad (16)$$

because $\tilde{g}_\lambda^e(V) = g_{V,e}^\lambda$ and $\tilde{\eta}_e = 0$.

4. Differential cross-section

The square of amplitude (16), after a number of transformations, can be represented in the form:

$$|\mathcal{M}^{\lambda_{p_1}, \lambda_{p_2}}(e^+ e^- \rightarrow \gamma, Z, Z' \rightarrow \bar{f} f)|^2 \\ = \sum_{\lambda_{k_1} = \pm} \sum_{\lambda_{k_2} = \pm} |\mathcal{M}_{\lambda_{k_1}, \lambda_{k_2}}^{\lambda_{p_1}, \lambda_{p_2}}|^2 = \delta_{\lambda_{p_2}, -\lambda_{p_1}} \\ \times \sum_{i,j=\gamma,Z,Z'} P_{ij}(s) G_e \left\{ \begin{matrix} \lambda_{p_1}, \lambda_{p_1} \\ i, j \end{matrix} \right\} \left[4g_v^f(i) g_v^f(j) \tilde{\eta}_f^2 \sin^2 \theta \right. \\ \left. + \tilde{G}_f \left\{ \begin{matrix} +, + \\ i, j \end{matrix} \right\} h_{p_1}^+ + \tilde{G}_f \left\{ \begin{matrix} -, - \\ i, j \end{matrix} \right\} h_{p_1}^- \right], \quad (17)$$

where

$$P_{ij}(s) = \frac{s^2((s - M_i^2)(s - M_j^2) + M_i\Gamma_i M_j\Gamma_j)}{((s - M_i^2)^2 + M_i^2\Gamma_i^2)((s - M_j^2)^2 + M_j^2\Gamma_j^2)}, \quad (18)$$

$$G_f \left\{ \begin{matrix} \lambda_1, \lambda_2 \\ i, j \end{matrix} \right\} = g_{i,f}^{\lambda_1} \times g_{j,f}^{\lambda_2}, \quad (19)$$

$$\tilde{G}_f \left\{ \begin{matrix} \lambda_1, \lambda_2 \\ i, j \end{matrix} \right\} = \tilde{g}_{\lambda_1}^f(i) \times \tilde{g}_{\lambda_2}^f(j), \quad (20)$$

$$h_{p_1}^\pm = (1 \pm \lambda_{p_1} \cos \theta)^2. \quad (21)$$

The differential scattering cross-sections of the processes $e_L^- e_R^+ \rightarrow f\bar{f}$ and $e_R^- e_L^+ \rightarrow f\bar{f}$ can be, respectively, written as:

$$\frac{d\sigma^{\text{LR}}}{dz} = \sum_{\lambda_{k_1} = \pm} \sum_{\lambda_{k_2} = \pm} \frac{d\sigma \left\{ \begin{matrix} -, + \\ \lambda_{k_1}, \lambda_{k_2} \end{matrix} \right\}}{dz}, \quad (22)$$

$$\frac{d\sigma^{\text{RL}}}{dz} = \sum_{\lambda_{k_1} = \pm} \sum_{\lambda_{k_2} = \pm} \frac{d\sigma \left\{ \begin{matrix} +, - \\ \lambda_{k_1}, \lambda_{k_2} \end{matrix} \right\}}{dz}. \quad (23)$$

where $z \equiv \cos \theta$.

After some transformations, we can find that the expressions (22) and (23) are written in the following form:

$$\frac{d\sigma^{\text{LR}}}{dz} = N_C \frac{\pi \alpha_{\text{em}}^2 \beta_f}{2s} \left[2\eta_f^2 q_{ef}^{SM+Z'} \left\{ \begin{matrix} -, - \\ -, + \end{matrix} \right\} + (1 - \beta_f z)^2 \times q_{ef}^{SM+Z'} \left\{ \begin{matrix} -, - \\ +, + \end{matrix} \right\} + (1 + \beta_f z)^2 q_{ef}^{SM+Z'} \left\{ \begin{matrix} -, - \\ -, - \end{matrix} \right\} \right], \quad (24)$$

$$\begin{aligned} \frac{d\sigma^{\text{RL}}}{dz} &= N_C \frac{\pi \alpha_{\text{em}}^2 \beta_f}{2s} \times \\ &\times \left[\eta_f^2 \left(q_{ef}^{SM+Z'} \left\{ \begin{matrix} +, + \\ -, + \end{matrix} \right\} + q_{ef}^{SM+Z'} \left\{ \begin{matrix} +, + \\ +, - \end{matrix} \right\} \right) + \right. \\ &\quad \left. + (1 + \beta_f z)^2 q_{ef}^{SM+Z'} \left\{ \begin{matrix} +, + \\ +, + \end{matrix} \right\} + \right. \\ &\quad \left. + (1 - \beta_f z)^2 q_{ef}^{SM+Z'} \left\{ \begin{matrix} +, + \\ -, - \end{matrix} \right\} \right]. \quad (25) \end{aligned}$$

where

$$\begin{aligned} q_{ef}^{SM+Z'} \left\{ \begin{matrix} \lambda_1, \lambda_2 \\ \bar{\lambda}_1, \bar{\lambda}_2 \end{matrix} \right\} &= \\ &= \sum_{i,j=\gamma,Z,Z'} P_{ij}(s) G_e \left\{ \begin{matrix} \lambda_1, \lambda_2 \\ i, j \end{matrix} \right\} G_f \left\{ \begin{matrix} \bar{\lambda}_1, \bar{\lambda}_2 \\ i, j \end{matrix} \right\}, \quad (26) \end{aligned}$$

and N_C is the color factor (1 for leptons and 3 for quarks) and α_{em} is the fine-structure constant.

If we take into account electron P_{e^-} and positron P_{e^+} polarization fraction, the differential cross-section can be written in the form:

$$\begin{aligned} \frac{d\sigma_{P_{e^-}, P_{e^+}}^{SM+Z'}}{dz} &= (1 - P_{e^-} P_{e^+}) \frac{1}{4} \\ &\times \left\{ (1 - P_{\text{eff}}) \frac{d\sigma^{\text{LR}}}{dz} + (1 + P_{\text{eff}}) \frac{d\sigma^{\text{RL}}}{dz} \right\}, \quad (27) \end{aligned}$$

$$P_{\text{eff}} = \frac{P_{e^-} - P_{e^+}}{1 - P_{e^-} P_{e^+}}, \quad (28)$$

where P_{eff} is the effective polarization.

Finally, by some manipulations, we can rewrite the (27) as:

$$\begin{aligned} \frac{d\sigma_{P_{e^-}, P_{e^+}}^{SM+Z'}}{dz} &= N_C (1 - P_{e^-} P_{e^+}) \frac{\pi \alpha_{\text{em}}^2 \beta_f}{8s} \left[Q_3^{SM+Z'} \right. \\ &\quad \left. + (1 - z\beta_f)^2 Q_1^{SM+Z'} + (1 + z\beta_f)^2 Q_2^{SM+Z'} \right], \quad (29) \end{aligned}$$

The linearity of $Q_{1,2,3}^{SM+Z'}$ is a crucial aspect of the technique presented in the Sec. 5.

It is important to note that effective parameters $Q_{1,2,3}^{SM+Z'}$ depend on polarization $p_{\text{eff}}^\pm = 1 \pm P_{\text{eff}}$ as follows:

$$\begin{aligned} Q_1^{SM+Z'} &= p_{\text{eff}}^- q_{ef}^{SM+Z'} \left\{ \begin{matrix} -, - \\ +, + \end{matrix} \right\} + p_{\text{eff}}^+ q_{ef}^{SM+Z'} \left\{ \begin{matrix} +, + \\ -, - \end{matrix} \right\}, \\ Q_2^{SM+Z'} &= p_{\text{eff}}^- q_{ef}^{SM+Z'} \left\{ \begin{matrix} -, - \\ -, + \end{matrix} \right\} + p_{\text{eff}}^+ q_{ef}^{SM+Z'} \left\{ \begin{matrix} +, + \\ +, + \end{matrix} \right\}, \\ Q_3^{SM+Z'} &= p_{\text{eff}}^- \left(q_{ef}^{SM+Z'} \left\{ \begin{matrix} -, - \\ -, + \end{matrix} \right\} + q_{ef}^{SM+Z'} \left\{ \begin{matrix} -, - \\ +, - \end{matrix} \right\} \right) + \\ &\quad + p_{\text{eff}}^+ \left(q_{ef}^{SM+Z'} \left\{ \begin{matrix} +, + \\ -, + \end{matrix} \right\} + q_{ef}^{SM+Z'} \left\{ \begin{matrix} +, + \\ +, - \end{matrix} \right\} \right), \quad (30) \end{aligned}$$

It is convenient to rewrite (30) in a more compact form:

$$\begin{aligned} Q_1^{SM+Z'} &= p_{\text{eff}}^- |q_{\text{LR}}^{SM+Z'}|^2 + p_{\text{eff}}^+ |q_{\text{RL}}^{SM+Z'}|^2, \\ Q_2^{SM+Z'} &= p_{\text{eff}}^- |q_{\text{LL}}^{SM+Z'}|^2 + p_{\text{eff}}^+ |q_{\text{RR}}^{SM+Z'}|^2, \\ Q_3^{SM+Z'} &= 2\eta_f^2 (p_{\text{eff}}^- \Re[q_{\text{LL}}^{SM+Z'} q_{\text{LR}}^{*SM+Z'}] \\ &\quad + p_{\text{eff}}^+ \Re[q_{\text{RL}}^{SM+Z'} q_{\text{RR}}^{*SM+Z'}]), \quad (31) \end{aligned}$$

where

$$q_{\lambda_e \lambda_f}^{SM+Z'} = \sum_{i=\gamma,Z,Z'} g_{i,e}^{\lambda_e} g_{i,f}^{\lambda_f} \frac{s}{s - M_i^2 + iM_i\Gamma_i}. \quad (32)$$

In the (32), indices λ_e and λ_f indicate the handedness of the initial electron and final fermion, respectively.

In case of $m_f \ll \sqrt{s}$, the expression (29) depends only on $Q_1^{SM+Z'}$ and $Q_2^{SM+Z'}$ effective parameters:

$$\frac{d\sigma_{P_{e^-}, P_{e^+}}^{SM+Z'}}{dz} = N_C(1 - P_{e^-} - P_{e^+}) \frac{\pi\alpha_{em}^2}{8s} \times \left[(1-z)^2 Q_1^{SM+Z'} + (1+z)^2 Q_2^{SM+Z'} \right]. \quad (33)$$

5. Model-independent technique

For the scenario $M_{Z'} \gg \sqrt{s}$, only the interference of the SM term with the Z' exchange is important. In this case the deviation from the SM prediction is given by:

$$\Delta Q_i(p_{\text{eff}}^-, p_{\text{eff}}^+) = Q_i^{SM+Z'} - Q_i^{SM}, \quad (i = 1, 2), \quad (34)$$

where

$$\Delta q_{\lambda_e \lambda_f} = |q_{\lambda_e \lambda_f}^{SM+Z'}|^2 - |q_{\lambda_e \lambda_f}^{SM}|^2. \quad (35)$$

As one can see, deviations $\Delta q_{\lambda_e \lambda_f}$ depend on the combination of λ_e and λ_f .

To obtain model-independent constraints on the $\Delta Q_{1,2}$ we use a χ^2 test. A Z' gives a signal in the observable O_i if the deviation ΔO_i from the SM prediction is more then experimental error δO_i . To extract confidence intervals on the $\Omega = \Delta Q_{1,2}$, we assume that the Ω follow an n -dimensional normal distribution ($i = 1, \dots, n$):

$$f(\Omega) = \frac{1}{(2\pi)^{n/2} |\tilde{V}|^{1/2}} \times \exp \left[-\frac{1}{2} (\Omega - \hat{\Omega})^T \tilde{V}^{-1} (\Omega - \hat{\Omega}) \right]. \quad (36)$$

Then, the square form

$$F(\Omega, \hat{\Omega}) = (\Omega - \hat{\Omega})^T \tilde{V}^{-1} (\Omega - \hat{\Omega}), \quad (37)$$

follow a χ^2 distribution [22].

For our case, optimal set $\hat{\Omega} = 0$ because the absence of ΔQ_i deviations implies that $Q_i^{SM+Z'} = Q_i^{SM}$.

In the square form (37), the covariance matrix \tilde{V} depend on the correlation coefficient ρ_{ij} and the standard deviations $\sigma_{i,j}$.

Subsequently, we can write the following statement:

$$\text{Prob} \left[F(\Omega, \hat{\Omega}) \leq K_\alpha^2 \right] = \alpha, \quad (38)$$

where K_α^2 is the quantile of the n -dimensional χ^2 distribution, which is defined by the integral:

$$\int_0^{K_\alpha^2} \frac{2^{-n/2}}{\Gamma(n/2)} \exp[-x/2] x^{n/2-1} dx = 1 - \alpha. \quad (39)$$

By (38), the equation for the confidence region of Ω for confidence level C.L. = $1 - \alpha$ can be written as:

$$F(\Omega, \hat{\Omega}) = K_\alpha^2 = \Delta\chi_{\text{crit}}^2, \quad (40)$$

therefore

$$\chi^2(\Omega) \approx \chi_{\text{min}}^2 + \Delta\chi_{\text{crit}}^2, \quad (41)$$

$$\chi_{\text{min}}^2 = \chi^2(\hat{\Omega}).$$

where $\chi_{\text{min}}^2 = 0$, $\Delta\chi_{\text{crit}}^2$ sets the confidence level (C.L.), typically 68.27% or 95%.

The range of Ω can be estimated by three probabilities:

1. The probability of being within the inscribed elliptical region ξ_1 ;
2. The probability of being within the described rectangular region ξ_2 . For such a case, the following probabilistic statement can be written as:

$$\text{Prob} \left[\hat{\Omega}_1 - K_\alpha \sigma_1 \leq \Omega_1 \leq \hat{\Omega}_1 + K_\alpha \sigma_1 \text{ and } \hat{\Omega}_2 - K_\alpha \sigma_2 \leq \Omega_2 \leq \hat{\Omega}_2 + K_\alpha \sigma_2 \right] = \xi_2. \quad (42)$$

The probabilistic content $\xi_2 > \xi_1$ and depends on ρ_{12} , which influences the shape and angle of the ellipse's inclination.

3. The probability of being within the horizontal strip ξ_3 , corresponding to the probabilistic statement:

$$\text{Prob} \left[\hat{\Omega}_1 - K_\alpha \sigma_1 \leq \Omega_1 \leq \hat{\Omega}_1 + K_\alpha \sigma_1 \text{ or } \hat{\Omega}_2 - K_\alpha \sigma_2 \leq \Omega_2 \leq \hat{\Omega}_2 + K_\alpha \sigma_2 \right] = \xi_3. \quad (43)$$

Often, correlation, particularly case 2, are not considered and only one-parameter intervals from case 3 are used. The case 3 can be used when the correlation is not significant, but it is important to understand that ξ_1 and ξ_3 are not equivalent.

As an observable we use the number of events $N_i^{SM+Z'}$ in the phase space z :

$$O_i \equiv N_i^{SM+Z'} = \mathcal{L}_{int} \cdot c_{pol} \cdot \varepsilon_f \cdot \int_{z_i}^{z_{i+1}} \left(\frac{d\sigma^{SM+Z'}}{dz} \right) dz, \quad (44)$$

where \mathcal{L}_{int} is the time-integrated luminosity, c_{pol} is a coefficient that depends on the electron and positron polarization, ε_f is the efficiency in the reconstruction and identification of fermions.

Due to the high luminosity, the number of events in the bin is relatively large and follows a Poisson distribution. Then, the random error is equal to $\sqrt{N_i^{SM}}$. If we take into account systematic uncertainty δ_{syst} , the experimental error is

$$\delta O_i \equiv \delta N_i^{SM} = \sqrt{N_i^{SM}(1 + \delta_{syst}^2 N_i^{SM})}, \quad (45)$$

After that, to extract confidence intervals on the Ω , we can write the χ^2 function as follows:

$$\chi^2(\Omega) = \sum_{i=1}^k \left[\frac{\Delta N_i(\Omega)}{\delta N_i^{SM}} \right]^2 \approx \chi_{\min}^2 + \Delta \chi_{\text{crit}}^2, \quad (46)$$

where $\Delta O_i \equiv \Delta N_i(\Omega) = N_i^{SM+Z'}(\Omega) - N_i^{SM}$ and k sets the number of bins for the angular distribution. It is not necessary to plot an ellipse in order to extract the confidence intervals [23]. Standard deviations and correlation coefficient can be derived from the equation. For example, after numerical calculation (45) we have an equation of the form:

$$C_{11}\Omega_1^2 + 2C_{12}\Omega_1\Omega_2 + C_{22}\Omega_2^2 + C_{33} = 0. \quad (47)$$

Using these C_{ij} coefficients it is possible to

calculate ρ_{12} and $\sigma_{1,2}$:

$$\rho_{12} = -\frac{C_{12}}{\sqrt{C_{11}C_{22}}}, \quad (48)$$

$$\sigma_1 = \frac{\sqrt{C_{11}}}{\sqrt{C_{11}C_{22} - C_{12}^2}}, \quad \sigma_2 = \frac{\sqrt{C_{22}}}{\sqrt{C_{11}C_{22} - C_{12}^2}}. \quad (49)$$

where

$$C_{11} = \sum_{i=1}^k \delta C_i^2 w_{i,-}^2, \quad C_{22} = \sum_{i=1}^k \delta C_i^2 w_{i,+}^2, \quad (50)$$

$$C_{12} = \sum_{i=1}^k \delta C_i^2 w_{i,-} w_{i,+}. \quad (51)$$

In these equations, δC_i is defined as:

$$\delta C_i = \frac{\mathcal{L}_{int} c_{pol} \varepsilon_f N_C (1 - P_e - P_{e+}) \pi \alpha_{em}^2}{\delta N_i^{SM}} \frac{1}{8s} \quad (52)$$

and

$$w_{i,\pm} = z_{i+1} \left(1 \pm z_{i+1} + \frac{z_{i+1}^2}{3} \right) - z_i \left(1 \pm z_i + \frac{z_i^2}{3} \right). \quad (53)$$

Analyzing the (48) and (49), we can conclude that the $\sigma_{1,2}$ and ρ_{12} are independent of the $\Delta \chi_{\text{crit}}^2 \equiv -C_{33}$.

By option of initial polarization, we have the opportunity to investigate two identical observables. In order to obtain confidence intervals on the deviation parameters (35), two numbers of events with different polarization shall be considered. As a result of this, we compose a system of equations and obtain the following solutions:

$$\Delta q_{LR} = \frac{p_{\text{eff}}^{+,b} \Delta Q_1^a - p_{\text{eff}}^{+,a} \Delta Q_1^b}{p_{\text{eff}}^{-,a} p_{\text{eff}}^{+,b} - p_{\text{eff}}^{+,a} p_{\text{eff}}^{-,b}},$$

$$\Delta q_{RL} = \frac{p_{\text{eff}}^{-,a} \Delta Q_1^b - p_{\text{eff}}^{-,b} \Delta Q_1^a}{p_{\text{eff}}^{-,a} p_{\text{eff}}^{+,b} - p_{\text{eff}}^{+,a} p_{\text{eff}}^{-,b}},$$

$$\Delta q_{LL} = \frac{p_{\text{eff}}^{+,b} \Delta Q_2^a - p_{\text{eff}}^{+,a} \Delta Q_2^b}{p_{\text{eff}}^{-,a} p_{\text{eff}}^{+,b} - p_{\text{eff}}^{+,a} p_{\text{eff}}^{-,b}},$$

$$\Delta q_{RR} = \frac{p_{\text{eff}}^{-,a} \Delta Q_2^b - p_{\text{eff}}^{-,b} \Delta Q_2^a}{p_{\text{eff}}^{-,a} p_{\text{eff}}^{+,b} - p_{\text{eff}}^{+,a} p_{\text{eff}}^{-,b}}, \quad (54)$$

where $\{a, b\} = \{P_{e^-} = \{a_1, b_1\}, P_{e^+} = \{a_2, b_2\}\}$.

These linear combinations also have normal distribution. Taking this into account, we calculate the (54) as:

$$|\Delta q_{\lambda_e \lambda_f}| = n_{\text{C.L.}} \sqrt{c_1^2 (\Delta Q_i^{\{a,b\}})^2 + c_2^2 (\Delta Q_i^{\{a,b\}})^2}. \quad (55)$$

where $n_{\text{C.L.}}$ sets the confidence level (1 for 68.27% C.L. and 1.96 for 95% C.L.) and the c_i^2 are coefficients from equations (54) that depend on combination of $p_{\text{eff}}^{\pm, \{a,b\}}$.

To extract the constraints on the Z' couplings, we assume that the total decay width is relatively large $\Gamma_{Z'} = 0.1 \times M_{Z'}$.

6. Numerical results

In this section we discuss the sensitivity of the process $e^+e^- \rightarrow \bar{f}f$ (where $f = \mu, \tau, b, c$) to the chirality λ_e and λ_f at CLIC. To this aim, we consider 2 stages with energies of the order of TeV (Table 1). For each of these stages, a baseline is adopted of sharing the running time for -80% and $+80\%$ electron polarization in the ratio 80:20 [1]. Then, the coefficient $c_{\text{pol}} = 1/5$ in the formula (44) is: $1/5$ for the $+80\%$ electron polarization, $4/5$ for the -80% electron polarization and 1 for unpolarized initial beams. We have chosen the polarization configurations $a = \{0, 0\}$ and $b = \{-0.8, 0\}$ in order to increase the total number of events.

Table 1: Baseline CLIC stages.

\sqrt{s} [TeV]	\mathcal{L}_{int} [ab $^{-1}$]		
	$P_{e^-} = 0\%$	$P_{e^-} = -80\%$	$P_{e^-} = +80\%$
1.5	2.5	2.0	0.5
3.0	5.0	4.0	1.0

For numerical calculation, we take into account the systematic uncertainty $\delta_{\text{syst}} = 2\%$ and assume that the identification efficiency are: 100% for $\mu^+\mu^-$ events, 50% for $\tau^+\tau^-$ events, 80% for $b\bar{b}$ events, 50% for $c\bar{c}$ events. The

region of the angular distribution at CLIC is bounded by the interval $[-1, 1]$ and divided by the number of bins $k = 20$ [1]. Since it is impossible to distinguish quark and anti-quark jets in the experiments, we have reduced the number of events in the process $e^+e^- \rightarrow \bar{q}q$ by half. Even so, the statistics of events for leptons and quarks are not significantly different because for quarks a color factor $N_C = 3$.

First of all, we calculate the $\sigma_{1,2}$ for the $\Delta Q_{1,2}^{a,b}$ which depend on the correlation coefficient (Tables 2 and 3). In our case, the correlation turned out to be negative and negligible.

Table 2. Standard deviations for $\Delta Q_{1,2}^{a,b}$ at CLIC with $\sqrt{s} = 1.5$ TeV ($\rho_{12} \approx -0.21$).

fermion	ΔQ_1^a	ΔQ_2^a	ΔQ_1^b	ΔQ_2^b
μ	∓ 0.0076	∓ 0.0146	∓ 0.0085	∓ 0.0168
τ	∓ 0.0106	∓ 0.0197	∓ 0.0119	∓ 0.0228
b	∓ 0.0025	∓ 0.0070	∓ 0.0030	∓ 0.0098
c	∓ 0.0049	∓ 0.0122	∓ 0.0065	∓ 0.0154

Table 3. Standard deviations for $\Delta Q_{1,2}^{a,b}$ at CLIC with $\sqrt{s} = 3$ TeV ($\rho_{12} \approx -0.21$).

fermion	ΔQ_1^a	ΔQ_2^a	ΔQ_1^b	ΔQ_2^b
μ	∓ 0.0106	∓ 0.0197	∓ 0.0119	∓ 0.0228
τ	∓ 0.0149	∓ 0.0272	∓ 0.0167	∓ 0.0315
b	∓ 0.0036	∓ 0.0097	∓ 0.0042	∓ 0.0135
c	∓ 0.0069	∓ 0.0168	∓ 0.0092	∓ 0.0213

In order to assess the sensitivity, using equations (54) and (55) we obtain model-independent constraints on the deviation $\Delta q_{\lambda_e \lambda_f}$ for all possible combinations of λ_e and λ_f . As shown in Tables 4 and 5, the process $e^+e^- \rightarrow \bar{f}f$ is the most sensitive to LR chiral combination.

Table 4. Model-independent constraints on the $\Delta q_{\lambda_e \lambda_f}$ at CLIC with $\sqrt{s} = 1.5$ TeV (68.27% C.L.).

fermion	Δq_{LR}	Δq_{RL}	Δq_{LL}	Δq_{RR}
μ	∓ 0.0054	∓ 0.0101	∓ 0.0107	∓ 0.0195
τ	∓ 0.0076	∓ 0.0141	∓ 0.0145	∓ 0.0264
b	∓ 0.0019	∓ 0.0034	∓ 0.0062	∓ 0.0100
c	∓ 0.0041	∓ 0.0068	∓ 0.0098	∓ 0.0167

Table 5. Model-independent constraints on the $\Delta q_{\lambda_e \lambda_f}$ at CLIC with $\sqrt{s} = 3$ TeV (68.27% C.L.).

fermion	Δq_{LR}	Δq_{RL}	Δq_{LL}	Δq_{RR}
μ	∓ 0.0076	∓ 0.0141	∓ 0.0145	∓ 0.0264
τ	∓ 0.0106	∓ 0.0197	∓ 0.0200	∓ 0.0364
b	∓ 0.0027	∓ 0.0048	∓ 0.0085	∓ 0.0138
c	∓ 0.0058	∓ 0.0096	∓ 0.0135	∓ 0.0231

To assess the sensitivity, we obtained allowed regions for the Z' couplings, shown in Figs. 2 and 3. The lines on these plots indicate the bounds of the allowed regions for different choices of λ_e and λ_f . To accomplish this, we use the assumption of the Z' total decay width, along with formula (35) and the explicit form given in (33). as shown in Figs. 2 and 3, the best sensitivity is observed for the LL chiral combination of the Z' couplings, which is attributed to the fact that the contribution of q_{LL}^{SM} in the formula (35) exceeds that of q_{LR}^{SM} .

Figs. 4 and 5 show how the regions depend for the product of $g_{Z',e}^L \times g_{Z',f}^L$ on the choice of the final state $\bar{f}f$. The best sensitivity occurs for b quarks, while the worst one is for τ leptons. This is related to the identification efficiency of $\tau^+\tau^-$ events, which is half that for $\mu^+\mu^-$ events. This difference is explained by the fact that for $\tau^+\tau^-$ events only hadronic decays are taken into account [1]. In the general case, it is possible to constrain only product of electron and fermion Z' couplings ($g_{Z',e}^{\lambda_e} \times g_{Z',f}^{\lambda_f}$). However, using the assumption of lepton universality for the Z' couplings, the process $e^+e^- \rightarrow \ell^+\ell^-$ has become unique. In this case, we can individually extract left- and right-handed lepton couplings of the Z' ($g_{Z',\ell}^L$ and $g_{Z',\ell}^R$). In this regard, the comparison of Z and Z' couplings is of some interest. The Tables 6 and 7 shows this comparison as the ratio $|g_{Z',\ell}^{\lambda_e}| / |g_{Z',\ell}^{\lambda_f}|$ for $M_{Z'}$ fixed at 5, 10 and 15 TeV.

 Table 6. Ratio of $|g_{Z',\ell}^{\lambda_e}| / |g_{Z',\ell}^{\lambda_f}|$ for $\ell = \mu$ at CLIC with $\sqrt{s} = 1.5$ TeV (68 % C.L.).

λ_ℓ	$M_{Z'} = 5$ TeV	$M_{Z'} = 10$ TeV	$M_{Z'} = 15$ TeV
L	3.4	1.7	1.1
R	1.9	0.9	0.6

 Table 7. Ratio of $|g_{Z',\ell}^{\lambda_e}| / |g_{Z',\ell}^{\lambda_f}|$ for $\ell = \mu$ at CLIC with $\sqrt{s} = 3$ TeV (68 % C.L.).

λ_ℓ	$M_{Z'} = 5$ TeV	$M_{Z'} = 10$ TeV	$M_{Z'} = 15$ TeV
L	7.0	2.9	1.9
R	3.9	1.7	1.1

Another interesting question is the potential of the process (3) to identify the $M_{Z'}$ by the measurement of the cross-section, which depends of the couplings of Z' and $M_{Z'}$. For this case, model-independent analysis can be employed in the context of a model-dependent analysis. If the model is given, i.e., we know the Z' couplings, it is possible to obtain constraints on the $M_{Z'}$.

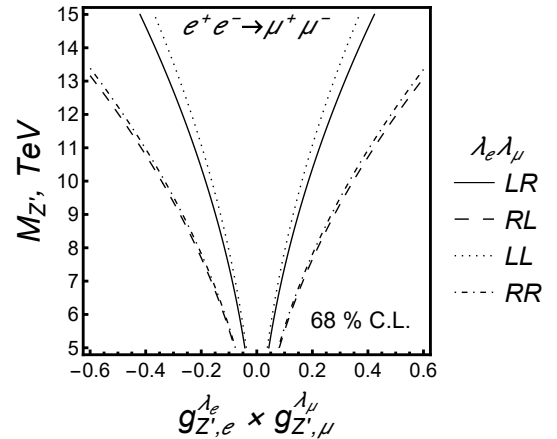


FIG. 2. Model-independent bounds on the product of electron and muon chiral couplings of the Z' in the $e^+e^- \rightarrow \mu^+\mu^-$ at CLIC [$\sqrt{s} = 1.5$ TeV, $\mathcal{L}_{int} = 2.5$ ab $^{-1}$ (unpolarized) and $\mathcal{L}_{int} = 2$ ab $^{-1}$ (polarized)] for 68.27 % C.L. (different line colors correspond to various choices of chiral combinations).

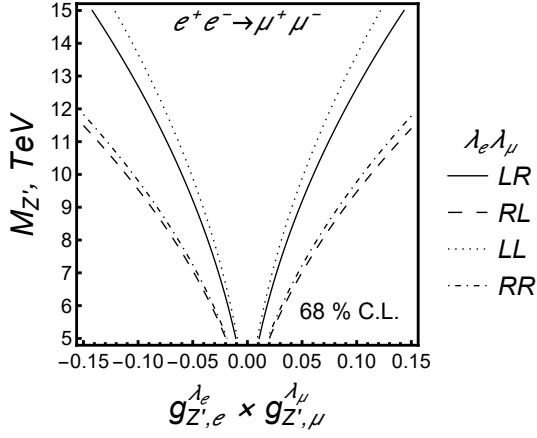


FIG. 3. Model-independent bounds on the product of electron and muon chiral couplings of the Z' in the $e^+e^- \rightarrow \mu^+\mu^-$ at CLIC [$\sqrt{s} = 3$ TeV, $\mathcal{L}_{int} = 5$ ab $^{-1}$ (unpolarized) and $\mathcal{L}_{int} = 4$ ab $^{-1}$ (polarized)] for 68.27 % C.L. (different line colors correspond to various choices of chiral combinations).

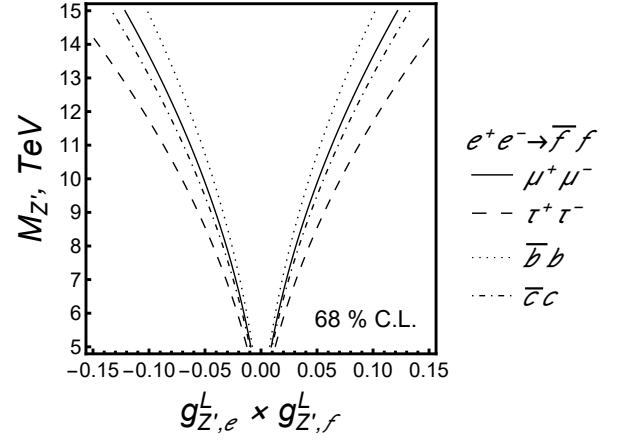


FIG. 5. Model-independent bounds on the product of electron and fermion chiral couplings of the Z' in the $e^+e^- \rightarrow \bar{f}f$ (where $f = \mu, \tau, b, c$) at CLIC [$\sqrt{s} = 3$ TeV, $\mathcal{L}_{int} = 5$ ab $^{-1}$ (unpolarized) and $\mathcal{L}_{int} = 4$ ab $^{-1}$ (polarized)] for 68 % C.L. (different line colors correspond to various choices of the final state).

7. Concluding remarks

The paper presents a technique for analyzing characteristics of an additional Z' -boson in the process $e^+e^- \rightarrow \bar{f}f$ (where $f \neq e$). This approach is based on the introduction of effective parameters (34), which depend on both the polarization of electron-positron beams and the characteristics of the Z' -boson. The linear dependence of the electron-positron annihilation cross-section on these effective parameters allows to obtain constraints using a combination of polarized observables. This technique makes it possible to obtain both model-independent and model-dependent constraints on the characteristics of the Z' -boson. The effective parameters allow to extract separate and model-independent information about individual lepton couplings of the Z' ($g_{Z',\ell}^L, g_{Z',\ell}^R$) under the assumption of lepton universality for a fixed $M_{Z'}$. In case of quark pair production, we can only constrain the product of electron and quark couplings of the Z' ($g_{Z',e}^{L,R} \times g_{Z',q}^{L,R}$).

By applying the technique, we obtained model-independent allowed regions for the mass and combinations of chiral couplings of the Z' -

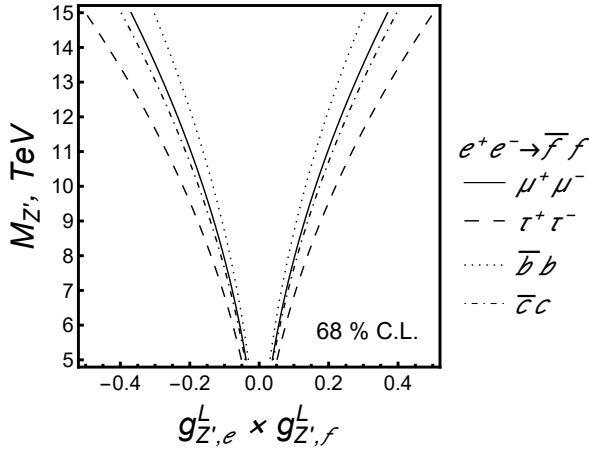


FIG. 4. Model-independent bounds on the product of electron and fermion chiral couplings of the Z' in the $e^+e^- \rightarrow \bar{f}f$ (where $f = \mu, \tau, b, c$) at CLIC [$\sqrt{s} = 1.5$ TeV, $\mathcal{L}_{int} = 2.5$ ab $^{-1}$ (unpolarized) and $\mathcal{L}_{int} = 2$ ab $^{-1}$ (polarized)] for 68.27 % C.L. (different line colors correspond to various choices of the final state).

boson for various final states ($f = \mu, \tau, b, c$) and high-energy stages at CLIC. The best sensitivity occurs for b quarks and μ leptons.

financial support.

Acknowledgements

The authors are grateful to the Belarusian Republican Foundation for Basic Research for

References

- [1] T.K. Charles *et al.* The Compact Linear Colider (CLIC) - 2018 Summary Report. CERN-2018-005-M, CERN-2018-005. Vol. 2/2018. (2018).
- [2] V. Abazov *et al.* Technical design report of the spin physics detector at NICA. [SPD Collaboration]. Natural Science Review. **1**, 325 (2024).
- [3] G. Weiglein *et al.* Physics interplay of the LHC and the ILC. [LHC/LC Study Group Collaboration]. Phys. Rept. **426**, 47-358 (2006).
- [4] A. Leike. The Phenomenology of extra neutral gauge bosons. Phys. Rept. **317**, 143-250 (1999).
- [5] P. Langacker. The physics of heavy Z' gauge bosons. Rev. Mod. Phys. **81**, 1199–1228 (2009).
- [6] S. Navas, *et al.* Review of particle physics. [Particle Data Group Collaboration]. Phys. Rev. D. **110**, 030001 (2024).
- [7] J.L. Hewett, T.G. Rizzo. Low-energy phenomenology of superstring-inspired E6 models. Physics Reports. **183**, 193-381 (1989).
- [8] F. Gursey, P. Ramond, P. Sikivie. A universal gauge theory model based on E6. Phys. Lett. B. **60**, 177-180 (1976).
- [9] M. Ashry, S. Khalil Phenomenological aspects of a TeV-scale alternative left-right model. Phys. Rev. D. **91**, 015009 (2015).
- [10] N. Arkani-Hamed, A.G. Cohen, E. Katz, A.E. Nelson. The Littlest Higgs. JHEP. **07**, 034 (2002).
- [11] T. Han, H.E. Logan, B. McElrath, L.-T. Wang. Phenomenology of the little Higgs model. Phys. Rev. D. **67**, 095004 (2003).
- [12] A. Gulov, Y. Moroz. Optimal observables for Z' models in annihilation leptonic processes. Phys. Rev. D. **98**, 115014 (2018).
- [13] V.M. Abazov *et al.* Search for a heavy neutral gauge boson in the dielectron channel with 5.4 fb^{-1} of $p\bar{p}$ collisions at $\sqrt{s} = 1.96$ TeV. [D0 Collaboration]. Phys. Lett. B. **695**, 88-94 (2011).
- [14] T. Aaltonen *et al.* Search for High Mass Resonances Decaying to Muon Pairs in $\sqrt{s} = 1.96$ TeV $p\bar{p}$ Collisions. [CDF Collaboration]. Phys. Rev. Lett. **106**, 121801 (2011).
- [15] G. Aad *et al.* Search for high-mass dilepton resonances using 139 fb^{-1} of $p\bar{p}$ collision data collected at $\sqrt{s} = 13$ TeV with the ATLAS detector. [ATLAS Collaboration]. Phys. Lett. B. **796**, 68-87 (2019).
- [16] Summary of Diboson Resonance Searches at the ATLAS experiment using full run-2 data. [ATLAS Collaboration]. ATL-PHYS-PUB-2023-007. (2023).
- [17] A. Das, P.S. Bhupal Dev, Y. Hosotani, S. Mandal. Probing the minimal U(1)X model at future electron-positron colliders via fermion pair-production channels. Phys. Rev. D. **105**, 115030 (2022).
- [18] A.A. Pankov, A.V. Tsytrinov, V.A. Bednyakov. High precision determination of $Z - Z'$ mixing in diboson production at the LHC. Int. J. Nonlin. Phenom. Complex Syst. **19**, 196-201 (2016).
- [19] A.A. Pankov, I.A. Serenkova, V.A. Bednyakov. Probing Z' boson in diboson production in semilepton final state with the ATLAS Data at the LHC at $\sqrt{s} = 13$ TeV. Int.J. Nonlin. Phenom. Complex Syst. **20**, 199-204 (2017).
- [20] A.A. Pankov, I.A. Serenkova, V.A. Bednyakov. Constraints on $Z - Z'$ mixing with ATLAS at the LHC at 13 TeV and 79.8 fb^{-1} . Int. J. Nonlin. Phenom. Complex Syst. **4**, 401-405 (2018).
- [21] V.V. Andreev. Calculation of Feynman diagrams using the blocks technique. Problems of physics,

- mathematics and technology. **1**(46), 7-12 (2014).
- [22] W.T. Eadie, D. Dryard, F.E. James, M. Roos, B. Sadoulet. *Statistical methods in experimental physics*. (North-Holland Publishing Company, Amsterdam, 1971).
- [23] D.V. Sinegribov, V.V. Andreev, I.A. Serenkova, V.R. Kurylenka. Model-independent constraints on effective parameters of extra neutral heavy bosons at future e^+e^- colliders. *Phys. Part. Nucl. Lett.* **21**, 658–660 (2024).